

Recent Observations of Clouds and Precipitation by the Airborne Precipitation Radar 2nd Generation in support of the GPM and ACE Missions

Stephen L. Durden*^a, Simone Tanelli^a, Eastwood Im^a

^aJet Propulsion Laboratory, California Institute of Technology, Pasadena, CA 91109

ABSTRACT

The Ku-/Ka-band, Doppler, scanning, polarimetric airborne radar, known as the Airborne Dual-Frequency Precipitation Radar (APR-2) has been collecting data since 2001 in support of many spaceborne instruments and missions aiming at the observation of clouds and precipitation (e.g., TRMM, AMSR-E, GPM, CloudSat, ACE). The APR-2 suite of processing and retrieval algorithms (ASPRA) produces Level 1 (L1) products, microphysical classification and retrievals, and wind intensity estimates. ASPRA was also generalized to operate on an arbitrary set of radar configuration parameters to study the expected performance of multi-frequency spaceborne cloud and precipitation radars such as the GPM DPR (Global Precipitation Measurement mission, Dual-Frequency Precipitation Radar) and a notional radar for the Aerosol/Clouds/Ecosystem (ACE) mission.

In this paper we illustrate the unique dataset collected during the Global Precipitation Measurement Cold-season Precipitation Experiment (GCPEX, US/Canada Jan/Feb 2012). We will focus on the significance of these observations for the development of algorithms for GPM and ACE, with particular attention to classification and retrievals of frozen and mixed phase hydrometeors.

Keywords: radar, precipitation, snow

1. INTRODUCTION

The Airborne 2nd Generation Precipitation Radar (APR-2) was developed by JPL under the NASA Instrument Incubator Program as a prototype for an advanced, dual-frequency spaceborne radar for a future spaceborne precipitation measurement mission [1]. Its development was motivated in part by the launch of the Tropical Rainfall Measuring Mission (TRMM) in 1997. The high quality data acquired by the Ku-band Precipitation Radar (PR) [2] on TRMM demonstrated the feasibility of making radar rainfall measurements from space. APR-2 is “second generation” in the sense that it expanded the PR’s capabilities and demonstrated new technology. Specifically, APR-2 is capable of making simultaneous measurements of rainfall parameters, including co-pol and cross-pol reflectivities and vertical Doppler velocities, at 13 and 35 GHz. The lower (Ku-band) frequency was chosen to match that of the Precipitation Radar (PR) on TRMM. The upper, Ka-band frequency was added to extend the system dynamic range to lower rain rates (only seen by Ka-band) and to provide dual-frequency data over a range of rain rates for improved retrievals. Furthermore, APR-2 also features several advanced technologies for performance improvement, including field-programmable gate array (FPGA) real-time data processing, low-sidelobe dual-frequency pulse compression, and dual-frequency scanning antenna. The APR-2 has successfully acquired data in the following field campaigns: the fourth Convection and Moisture Experiment (CAMEX-4) in the tropical Atlantic Ocean (2001) [3]; the Wakasa Bay Experiment for Aqua validation in 2003; flights over the US west coast, Gulf of Mexico and coastal regions in 2003; the NASA African Monsoon Multidisciplinary Analyses (NAMMA) in the eastern Atlantic and west coast of Africa during 2006 [4], the Tropical Composition, Cloud and Climate Coupling (TC4) experiment in the eastern Pacific, Caribbean, central and south America in 2007 [5]; the hurricane Genesis and Rapid Intensification (GRIP) experiment in tropical systems and hurricanes (2010); and, most recently, the Global Precipitation Measurement (GPM) mission Cold-season Precipitation Experiment (GCPEX) over an instrumented ground site in Canada, in early 2012. APR-2 was designed for operation on the NASA DC-8 aircraft but also operated on the NASA P-3 aircraft for the Wakasa Bay data collection.

[*sdurden@jpl.nasa.gov](mailto:sdurden@jpl.nasa.gov); phone 818-354-4719; fax 818-3936440

The GPM mission is a follow-on to the highly successful TRMM. While TRMM has used a Ku-band Precipitation Radar (PR) to observe rainfall over the tropics, GPM will carry a Dual-frequency (13/35 GHz) Precipitation Radar (DPR) [6] for measurement of precipitation over both the tropics and mid-latitudes. Because of the use of both Ku-band and Ka-band radar frequencies and the observation of mid-latitude precipitation (e.g., snowfall), new algorithms are needed for retrieving precipitation from the GPM DPR measurements. In preparation for GPM, several field experiments have been carried out to acquire data useful for algorithm development; these include the Mid-latitude Continental Convective Clouds Experiment (MC3E), the Light Precipitation Verification Experiment (LPVEx), and GCPEX, mentioned above. GCPEX used the NASA DC-8 aircraft with both the APR-2 and a multichannel microwave radiometer. In addition to the DC-8, a Citation aircraft flew at lower levels to make in situ measurements of the clouds and precipitation being remotely sensed by the DC-8. Most of the flights were over a ground location at Egbert, Ontario, allowing ground-based in situ measurements of precipitation characteristics. Furthermore, APR-2 itself acquires data that can assist in constraining retrievals and improving their accuracy. For example, the DPR on GPM does not have Doppler or dual-polarization capabilities, but APR-2 does. While dual-polarization can allow better classification of precipitation (e.g., rain, snow, melting ice, etc), the Doppler velocity also enhances particle identification and can be useful in looking at atmospheric dynamics. Beyond GPM, the National Research Council Decadal Survey recommended the Aerosol/Cloud/Ecosystems (ACE) mission [7]. This mission would also have a dual-frequency radar that would use Ka-band for light precipitation and clouds and W-band for clouds. While the frequency set differs from APR-2, the dual-frequency retrieval techniques developed for APR-2 data can be applied to ACE, as can insights gained about cloud microphysics and Ka-band scattering. This paper describes the APR-2 data and processing and then shows preliminary results from our ongoing analysis of data from GCPEX.

2. APR-2 DESCRIPTION

The APR-2 operational geometry is illustrated in Figure 1, while Table 1 shows the APR-2 operating parameters. APR-2 usually is operated on the NASA DC-8 aircraft, although the Wakasa Bay experiment in 2003 was performed using the NASA P-3 aircraft. More details are provided in Sadowy et al. (2003). The APR-2 instrument is more than 10 years old. Starting with the GRIP deployment in 2010 several upgrades have been planned and some completed, including a new radome (GRIP) and a new 35 GHz high-power amplifier (GCPEX). The new radome was specifically designed for dual-frequency operation and has very low loss and low reflection at both frequencies. The new amplifier increased output power at Ka-band, yielding an improved 35 GHz sensitivity. This was of prime importance for GCPEX, since the target weather systems (snow) had low reflectivity.

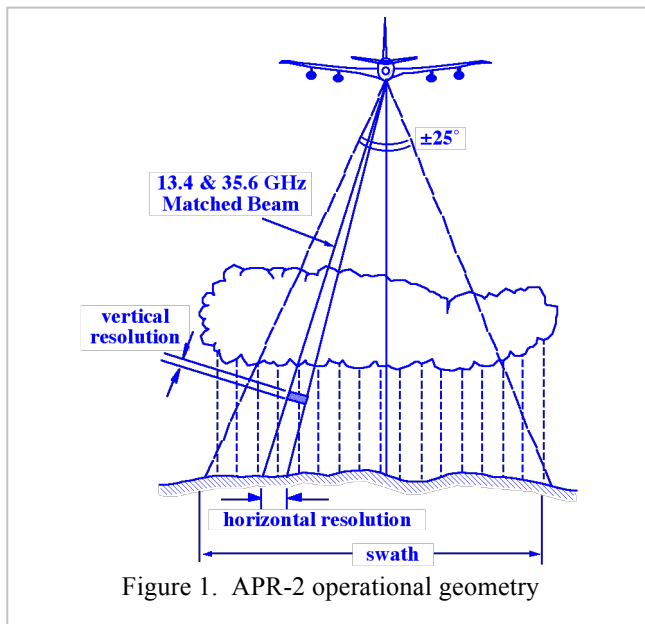


Figure 1. APR-2 operational geometry

Table 1. APR-2 GCPEX Parameters

Parameters	Ku-band	Ka-band
Frequency	13.4 GHz	35.6 GHz
Polarization	HH, HV	HH, HV
Antenna diam	0.4 m	0.14 m
Antenna sidelobe	-30 dB	-30 dB
Antenna scan angle	±25°	±25°
Peak power	200 W	200 W
Bandwidth	4 MHz	4 MHz
Pulsewidth	10 μs	10 μs
PRF	5 kHz	5 kHz
Vertical resolution	60 m	60 m
Horiz. resol. (@ 10 km alt.)	800 m	1000 m
Ground Swath	10 km	10 km
Sensitivity (@ 10 km range)	10 dBZ	-10 dBZ
Doppler precision	0.3 m/s	1 m/s

3. APR-2 DATA PROCESSING

The APR-2 suite of processing and retrieval algorithms (ASPRA) handles all the data processing. Raw radar data are first processed to obtain reflectivity, linear depolarization ratio (LDR), and Doppler velocity measurements. The conversion to reflectivity makes use of transmit power coupled to the receiver via a calibration loop. Using one-time measurements of loop losses and real-time measurements of the receiver output during the transmit event, the received power can be calibrated and multiplied by the range-squared to yield reflectivity. The resulting dataset is then processed iteratively to accurately estimate the true aircraft navigation parameters and to classify the surface return. These intermediate products are used to refine reflectivity and LDR calibrations (by analyzing clear air ocean surface returns), and to correct Doppler measurements for the aircraft motion. The standard approach to correcting for the aircraft motion is to examine the Doppler for the surface, which is normally entirely dominated by the aircraft motion. In a number of experiments other instruments on the DC-8 have acquired high-accuracy navigation data. We have used these to directly estimate the antenna pointing and Doppler correction. Comparison with the method of using the surface Doppler shows that the two methods generally agree quite well. One possible exception is inside hurricanes, where high winds can induce a surface current that is large enough to create discrepancies between the surface Doppler and the calculated Doppler of a few m/s.

The Ku-band calibration is verified using observations of the ocean surface in clear air conditions [8]. This technique has been used previously in calibrating data from the JPL Ku-band airborne rain radar ARMAR [9], since the ocean backscatter near 10° incidence is known to be relatively independent of surface wind speed. APR-2 data are adjusted so that clear ocean returns have an average normalized radar cross section of 7.1 dB at 10° , which is comparable to those obtained by several models, previous experiments and missions (e.g., SASS-2 [10], AAFE-RADSCAT [11], TRMM [12]). The APR-2 Ku-band channel calibration accuracy is therefore estimated to be within roughly 1 dB. Ocean backscatter at Ka-band is much less well characterized. Although calculations with the two-scale electromagnetic (EM) model that was described in [13] show similar behavior to Ku-band, previous measurements are scarce and show disagreements as large as 6 dB [14], [15]. Because of this limitation, a different technique was used to validate the APR-2 Ka-band calibration. This technique relies on comparing the Ka-band returns from small drops (nearly Rayleigh scatterers) at the top of a stratiform rain layer to the corresponding Ku-band returns whose calibration has been verified using the ocean method just described. Within the Rayleigh regime, the equivalent reflectivity factors Z_e at these two frequencies are equal. In practice, we also need to account for atmospheric gas attenuation, melting layer attenuation, and non-Rayleigh effects. An automated procedure was developed to select suitable portions of the dataset (i.e., the topmost 300 m of light rain below thin melting layers) and to extract the statistics of reflectivity. Overall, the calibration uncertainty in Ka- relative to Ku-band is about 1-2 dB, due to the aforementioned approximations and residual quantization errors. The Ku- and Ka-band antenna beams are generated from a single dual-frequency feedhorn. The co-alignment of the maximum directivity directions for the two beams has been verified in laboratory tests. Although much of the precipitation in GCPEX was snow, there were cases of light, stratiform liquid precipitation, allowing the technique to be applied to the GCPEX dataset.

Level 2 processing of selected data begins with the calibrated and Doppler-corrected Level 1 data. The melting layer of precipitation is detected and its boundaries and characteristics are identified at the APR-2 range resolution of approximately 60 m. For precipitation retrievals, we now use an improved dual-frequency algorithm, relative to our previous algorithm described in [16]. The new algorithm takes as input radar reflectivities at both frequencies when available, Doppler velocity, and LDR. It also uses an initial, deterministic classification based on these parameters and an estimate of path-integrated attenuation (PIA) at each frequency, if available. The retrieval algorithm takes a fully Bayesian approach, performing multiple retrievals by perturbing PIA and *a priori* mean particle size assumptions. The particle size distribution is assumed to be a gamma-distribution, with parameters selected to be statistically uncorrelated. The algorithm allows both liquid water and various forms of ice. Fractional populations of liquid, snow, graupel, and other ice are refined based upon the model of Rasmussen and Heymsfield [17]. In keeping with the Bayesian approach, the final estimate is a weighted average based on several performance measures. Figure 2 shows an example of retrievals in a hurricane (Earl, on September 1, 2010). The retrieval takes advantage of the ratio of Ku-band to Ka-band reflectivity, the Dual-wavelength Ratio (DWR) at lower left. In areas with small particles and little attenuation, we expect the DWR to be near zero, since particles would be in the Rayleigh-scattering regime at both frequencies. For larger particles, the DWR increases, since non-Rayleigh effects reduce the reflectivity at Ka-band. Hence, the magnitude of DWR relates to particle size and enables more accurate particle size retrieval using the dual-frequency APR-2 data.

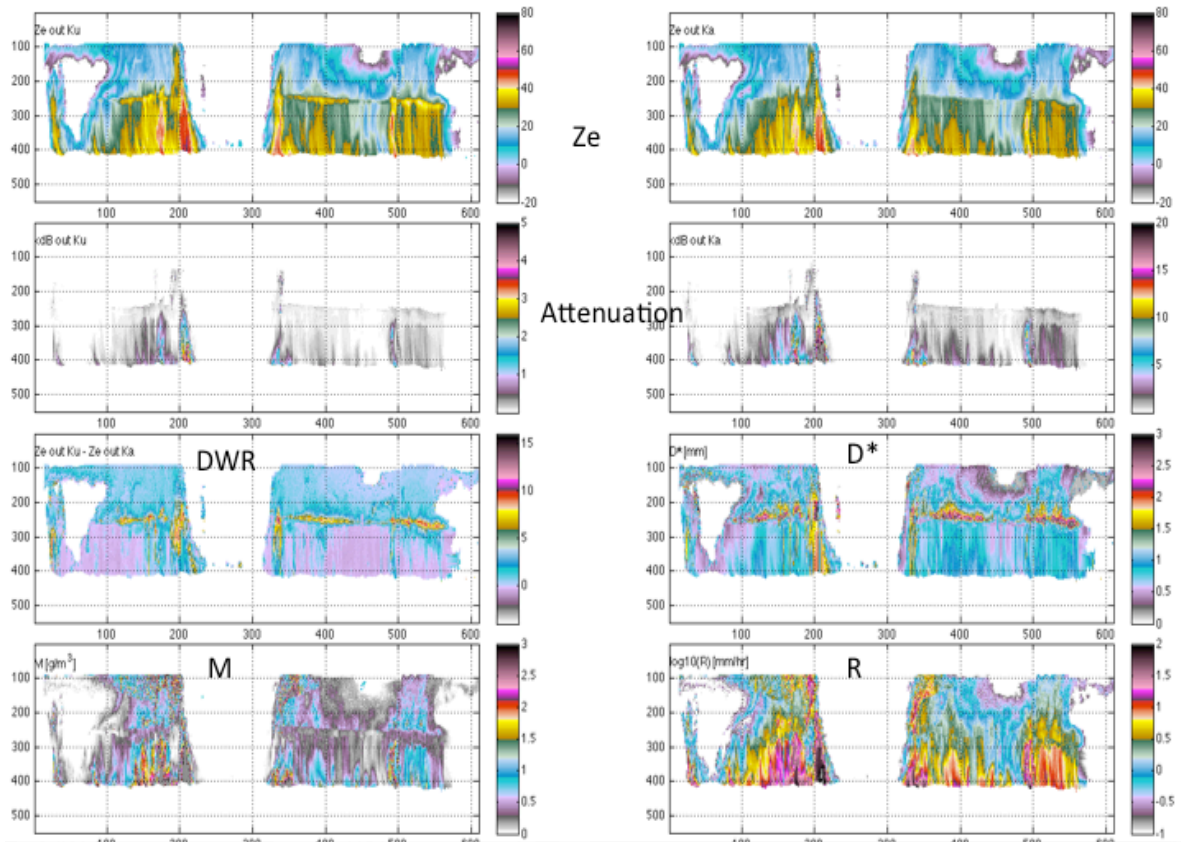


Figure 2. Example of precipitation retrieval using APR-2 data in a tropical cyclone. The top four panels show the vertical slices through the storm (center gap is eye). The panels are corrected reflectivity Z_e and the specific attenuation at Ku-band (left) and Ka-band (right). The corrected Z_e is that reflectivity which would be measured with no attenuation present. The lower panels show the dual-wavelength ratio (DWR), corrected for attenuation, the mass-weighted mean particle size D^* , the water content M , and the rainrate R .

4. GCPEX DATA ANALYSES

GCPEX took place in January and February 2012. The instrumented ground site near Egbert, Canada is an atmospheric research facility operated by the Air Quality Research Branch of the Meteorological Service of Canada. The objective of overflying all of these instruments was to have independent measurements of falling snow water equivalent rates, snow pack water equivalent, microwave surface emission properties, particle size distributions (PSD's), snowfall bulk density and snow particle habits. These ground-based measurements will be used in validating assumptions built into the retrieval algorithms (such as described in the previous section), as well validating the estimated snowfall rate and particle size output by the algorithms for specific cases. This section summarizes the APR-2 data acquired in this experiment, provides statistics on various APR-2 measurements, and then discusses an example of applying the retrieval algorithm described above to GCPEX data.

4.1 Overview of APR-2 Operations in GCPEX

APR-2 collected data on 16 local science flights beginning January 19, 2012, with the last science flight on February 24, 2012. Each flight lasted a few hours, with approximately 45 minutes ferry time from the DC-8's base to the experiment

site. Figure 3 shows an example of the flight track covering the experiment area. In spite of being during the midpoint of the typical winter storm season, temperatures during most of GCPEX were well above normal, as was the case over much of North America. This lessened the intensity of the winter storms resulting in more systems with mixed phase and rain at the surface and more systems with light snow.

4.2 APR-2 Data Characteristics

The APR-2 data for GCPEX was processed and calibrated as described in Section 2. It generally appears to be of good quality. As snowfall was generally light to moderate, the highest reflectivities were encountered in liquid precipitation events, easily recognized by the presence of a bright band at the height of the zero-degree isotherm. As the large snow particles melt, they become wet, enhancing their reflectivity. Once melting completes, the particles collapse and accelerate, reducing reflectivity. This leads to enhanced reflectivity near the freezing level. When the surface temperature is below freezing, no such layer is seen. Since ice clouds with melting precipitation are seen even in the tropics, our initial focus on GCPEX has been data from the events with sub-freezing surface temperatures, so that only snow or other forms of solid precipitation are present. Figure 4 (left panel) shows a scatter plot of DWR versus Ku-band reflectivity Z_e over the entire experiment. The data were taken from an altitude of about 1-2 km. Reflectivities extend from near -20 dBZ up to 30 dBZ in the heavier snow storms. The DWR is observed from 0 dB to over 12 dB. The large scatter shows that even low reflectivity particles can sometimes have large DWR. This indicated that the same reflectivity can correspond to a variety of mean particle sizes and, hence, mean snowfall rates. Thus, single frequency snowfall retrievals would be subject to large errors; a mean particle size would have to be assumed *a priori*, rather than retrieved using the DWR.

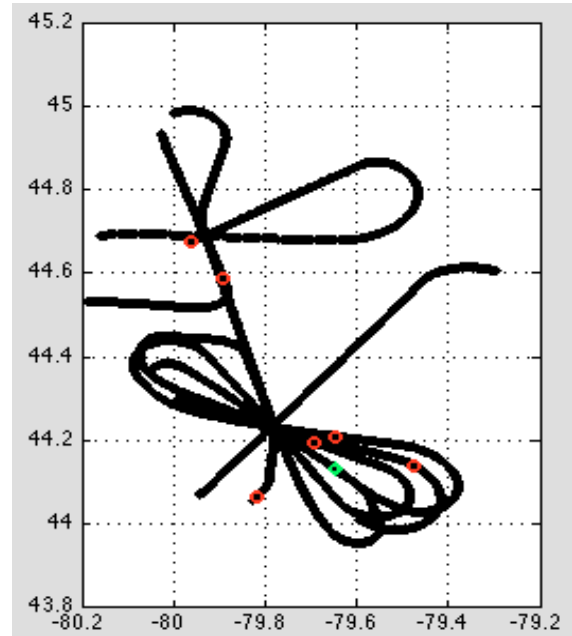


Figure 3. Example of DC-8 flight track in GCPEX.

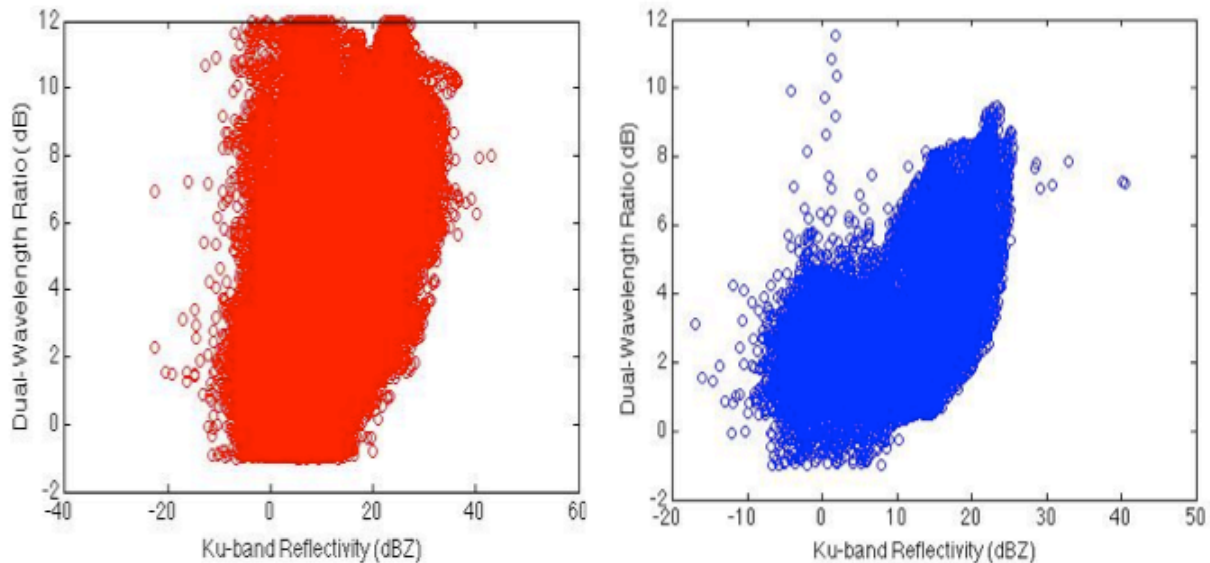


Figure 4. At left is scatter plot of DWR versus Ku-band Z_e over the entire experiment. Values are derived from a layer 1-2 km above the surface. At right is the same type of data as at left but only for the flight of January 28.

In the right panel of Figure 4, we show the same information for a single flight over the ground site, on January 28. The shape of the scatter plot is rather different from that for the entire experiment, and the ranges of both reflectivity and DWR are more limited than for the full experiment. On this particular day, the microphysical processes underlying the snowfall created smaller particles, especially at the lower reflectivities. On other days, even the low reflectivity particles were large, e.g., large, dry snow particles, filling in the upper left portion of the scatter.

4.3 Preliminary Snowfall Retrieval Example

We applied the dual-frequency retrieval algorithm described in Section 3 to a snowfall case from January 28. The observed radar data are shown in Figure 5. As described in the caption, these are the so-called level 1 data that are input to the algorithm. The measured DWR is small, except very close to the surface and near the end of the data, at right. Most of these data were taken over water; the area at right with the larger particles was over land, and this appears to be a case of lake-effect snow. Figure 6 shows the results of applying the retrieval to the data in Figure 5. The Ku-band reflectivity in this case is the true reflectivity that would be observed if no attenuation were present. In this particular case, attenuation is small, especially at Ku-band, so the output reflectivity is very close to the input. The mass

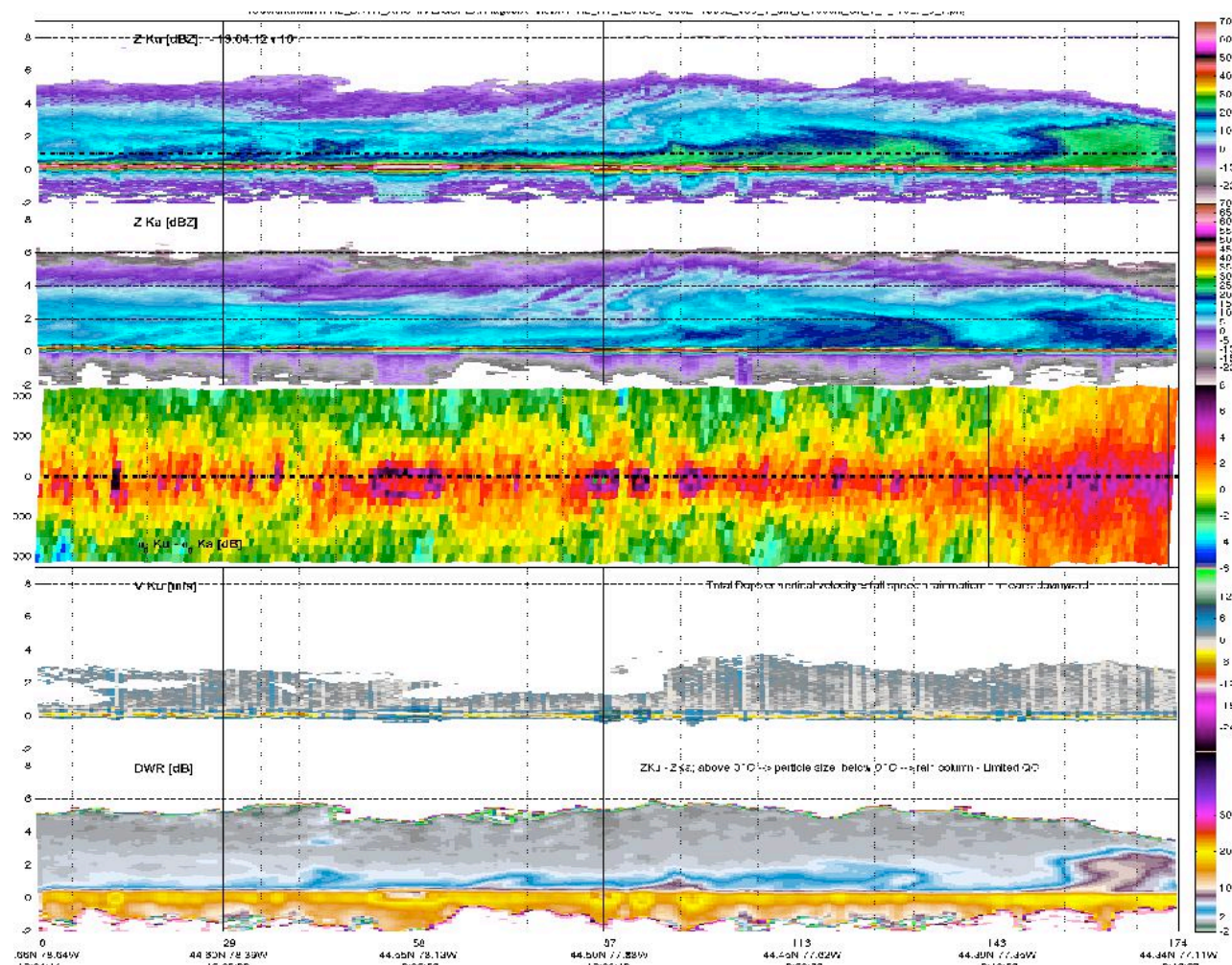


Figure 5. APR-2 data acquired over snowfall, January 28, 2012. The top panel is a vertical slice along the flight track of the Ku-band reflectivity. Echoes extend up to an altitude of about 5-6 km. The next panel is a vertical slice of Ka-band reflectivity, then a horizontal slice showing the difference in surface backscatter between the two frequencies. The panel next to the lowest is the measured Doppler velocity, and the last panel is the DWR.

concentration and snowfall rate (melted equivalent) are consistent with light snow, as was observed on the ground; the peak snowfall rate is a few mm/h. Most of these data correspond to small particles (size < 2 mm). The area at the end of the data over land, however, has larger mean particle size (up to near 4 mm), consistent with the large DWR in this area. Using only single frequency data, the mean particle size is assumed constant, so the change in particle size would have resulted in an error in the retrieved snowfall rate, as noted previously.

5. SUMMARY AND CONCLUSIONS

We have provided a brief overview of the APR-2 Ku/Ka-band dual-frequency radar and its data processing, calibration, and Bayesian precipitation retrieval algorithms. APR-2 acquired high-quality data during the GCPEX experiment, as part of the pre-launch GPM validation activities. The data from GCPEX will be used to better understand snowfall and its signature at Ku- and Ka-bands. This understanding will be directly used in radar retrieval algorithms for GPM and in algorithm validation, since extensive surface data was collected in parallel with the APR-2 data. Longer term, the data should be useful in assessing performance of various instrument designs for the planned ACE mission.

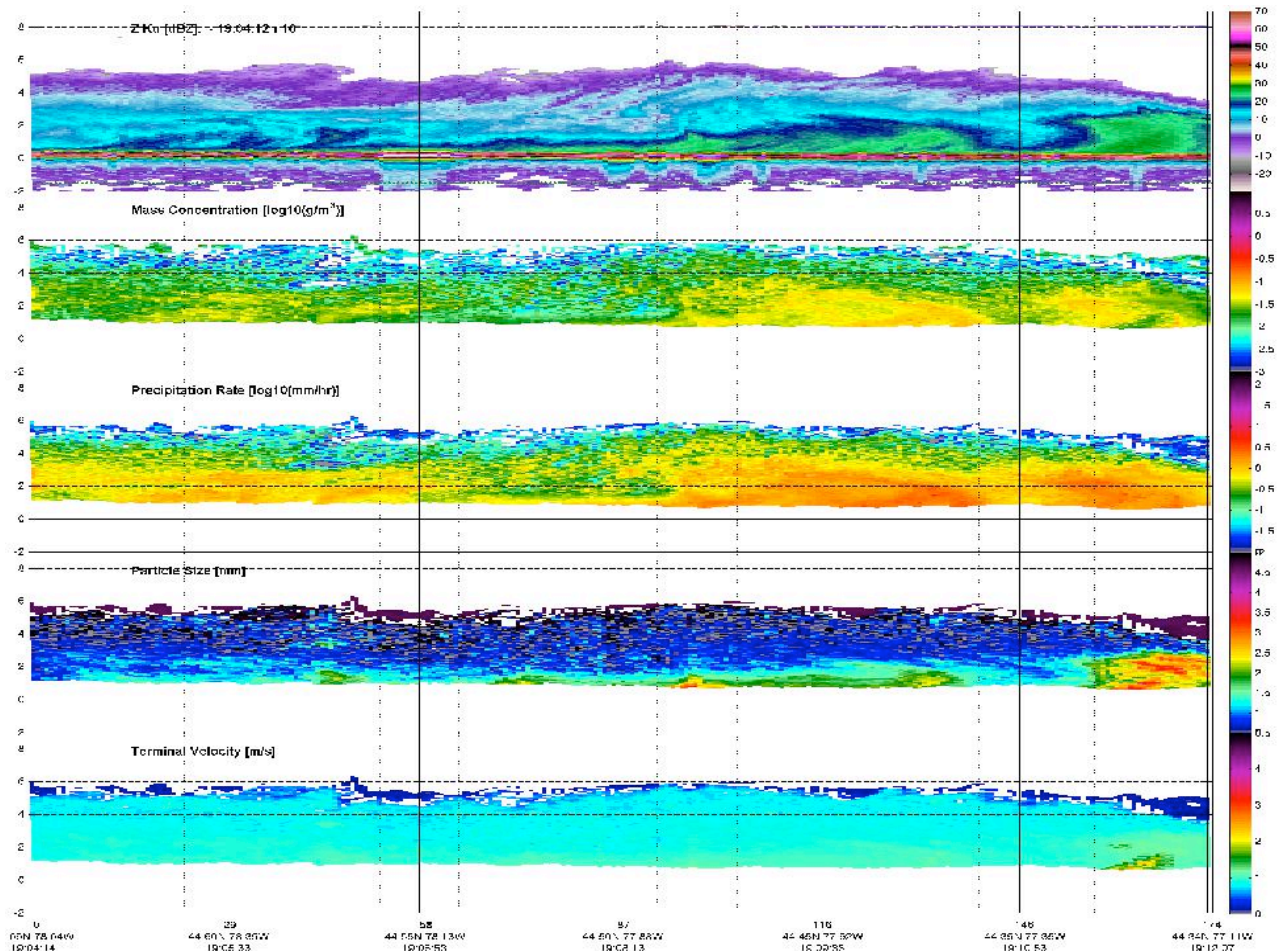


Figure 6. Outputs of the dual-frequency retrieval algorithm, plotted versus altitude and along-track distance. The top panel is the Ku-band reflectivity after correction for attenuation (which is generally small in this case). The second panel from the top is the mass concentration of ice in g/m³. Next is the liquid equivalent precipitation rate in mm/h, the mean particle size in cm, and the terminal velocity in m/s. The air motion can be estimated by removing the terminal velocity from the total measured velocity in Figure 5.

ACKNOWLEDGEMENTS

The research described in this paper was carried out at the Jet Propulsion Laboratory, California Institute of Technology, under contract with the National Aeronautics and Space Administration.

REFERENCES

- [1] Sadowy, G. A., Berkun, A. C., Chun, W., Im, E., and Durden, S. L., "Development of an advanced airborne precipitation radar," *Microwave J.*, 46, 84-98 (2003).
- [2] Kozu, T., et al., "Development of precipitation radar onboard the Tropical Rainfall Measuring Mission (TRMM) satellite," *IEEE Trans. Geosci. Remote Sens.*, 39, 102-116 (2001).
- [3] Kakar, R., Goodman, M., Hood, R., Guillory, A., "Overview of the Convection and Moisture Experiment (CAMEX)," *J. Atmos. Sci.*, **63**, 5-18 (2006).
- [4] Zipser E. J., et al., "The Saharan Air Layer and the Fate of African Easterly Waves - NASA's AMMA 2006 Field Program to Study Tropical Cyclogenesis: NAMMA," *Bull. Am. Met. Soc.*, 90, 1137-1156 (2009).
- [5] Jensen, E. J., Lawson, P., Baker, B., Pilson, B., Mo, Q., Heymsfield, A. J., Bansemer, A., Bui, T.P., McGill, M., Hlavka, D., Heymsfield, G., Platnick, S., Arnold, G. T., and Tanelli, S., "On the importance of small ice crystals in tropical anvil cirrus," *Atmos. Chem. Phys. Discuss.*, 9, 5321-5370 (2009).
- [6] Senbokuya, Y., et al., "Development of the spaceborne dual-frequency precipitation radar for the Global Precipitation Measurement mission," in *Proc. IGARSS*, 3566-3569 (2004).
- [7] NRC (National Research Council), *Earth Science and Applications from Space: National Imperatives for the Next Decade and Beyond*, (2007).
- [8] Tanelli, S., Durden, S. L., and Im, E., "Simultaneous measurements of Ku- and Ka-band sea surface cross-sections by an airborne radar," *IEEE Geosci. Remote Sens. Lett.*, 3, 359-363 (2006).
- [9] Durden, S. L., Im, E., Li, F. K., Ricketts, W., Tanner, A., and Wilson, W., "ARMAR: An airborne rain mapping radar," *J. Atmos. Oceanic Technol.*, 11, 727-737 (1994).
- [10] Wentz, F., Peteherych, S., and Thomas, L. A., "A model function for ocean radar cross section at 14.6 GHz," *J. Geophys. Res.*, 89, 3689-3704 (1984).
- [11] Schroeder, L. C., Schaffner, P. R., Mitchell, J. L., and Jones, W. L., "AAFE RADSCAT 13.9-GHz measurements and analysis: Wind-speed signature of the ocean," *IEEE J. Oceanic Eng.*, 10, 346-357 (1985).
- [12] Freilich, M. H., and Vanhoff, B. A., "The relationship between winds, surface roughness, and radar backscatter at low incidence angles from TRMM precipitation radar measurements," *J. Atmos. Oceanic Technol.*, 20, 549-562 (2003).
- [13] Masuko, H., Okamoto, K., Shimada, M., and Niwa, S., "Measurement of microwave backscattering signatures of the ocean surface using X-band and Ka band airborne scatterometers," *J. Geophys. Res.*, 91, 13065-13083, 1986.
- [14] Vandemark, D., Chapron, B., Sun, J., Crescenti, G. H., and Graber, H. C., "Ocean wave slope observations using radar backscatter and laser altimeters," *J. Phys. Oceanogr.*, 34, 2825-2841, 2004.
- [15] Durden, S. L., and Vesecky, J. F., "A physical radar cross-section model for a wind-driven sea with swell," *IEEE J. Ocean. Eng.*, 10, 445-451, (1985).
- [16] Haddad, Z. S., Meagher, J. P., Durden, S. L., Smith, E. A., and Im, E., "Drop size ambiguities in the retrieval of precipitation profiles from dual-frequency radar measurements," *J. Atmos. Sci.*, 63, 204-217 (2006).
- [17] Rasmussen, R. M., and Heymsfield, A. J., "Melting and shedding of graupel and hail. Part I: Model physics," *J. Atmos. Sci.*, 44, 2754-2763 (1987).